Electron transport via polaron hopping in bulk TiO_2: A density functional theory characterization

N. Aaron Deskins and Michel Dupuis
Chemical Sciences Division, Pacific Northwest National Laboratory, Battelle Boulevard, K1-83, Richland, Washington 99354, USA
(Received 20 October 2006; revised manuscript received 22 March 2007; published 22 May 2007)

This work focuses on the intrinsic electron transport in stoichiometric TiO_2. Electron hopping is described by a polaron model, whereby a negative polaron is localized at a Ti^{3+} site and hops to an adjacent Ti^{4+} site. Polaron hopping is described via Marcus theory formulated for polaronic systems and quasiequivalent to the Emin-Holstein-Austin-Mott theory. We obtain the relevant parameters in the theory (namely, the activation energy ΔG^*, the reorganization energy λ, and the electronic coupling matrix elements V_{AB}) for selected crystallographic directions in rutile and anatase, using periodic density functional theory (DFT)+U and Hartree-Fock cluster calculations. The DFT+U method was required to correct the well-known electron self-interaction error in DFT for the calculation of polaronic wave functions. Our results give nonadiabatic activation energies of similar magnitude in rutile and anatase, all near ~0.3 eV. The electronic coupling matrix element V_{AB} was determined to be largest for polaron hopping parallel to the c direction in rutile and indicative of adiabatic transfer (thermal hopping mechanism) with a value of 0.20 eV, while the other directions investigated in both rutile and anatase gave V_{AB} values of about one order of magnitude smaller and indicative of diabatic transfer (tunneling mechanism) in anatase.

DOI: 10.1103/PhysRevB.75.195212 PACS number(s): 71.38.Ht, 72.20.Ee, 71.20.Nr, 72.80.Ga

I. INTRODUCTION

Titania, TiO_2, is one of the most studied photoactive materials and has been used for a large variety of purposes, including pollutant degradation[1,2] and solar energy production.[3] Efficient utilization of solar energy for both catalytic purposes and energy production is a promising area of research to contribute to meeting the energy needs of tomorrow. Toward this goal, better understanding and design of photoactive compounds are needed, including understanding the transport of e^-/h^+ in semiconductor materials. Additionally, electrons and holes typically interact with surface-adsorbed species and perform a vital role in photocatalysis.

TiO_2 is able to adsorb photons, leading to excitation of valence electrons to conduction states. In the process, positively charged holes are also created. These electrons and holes can migrate through the crystal to react with surface-adsorbed species to become trapped at defect sites, to travel through an electric circuit to create electricity, or to recombine to form ground-state structures. The excited conduction electrons in TiO_2 have historically been described by several authors[4–6] using a small-polaron model. Recent experimental work[7,8] as well as theoretical work[9,10] also add validity to the polaron model. In the polaron model, a conduction electron localizes at a site, or atom, in the system and causes a lattice distortion which stabilizes (traps) the localized electron. This electron migrates from site to site via a hopping mechanism, primarily through thermal motion. In the case of TiO_2, electrons localize at Ti^{4+} sites to form Ti^{3+}.

The common forms of titania, rutile and anatase, are both photocatalytically active with anatase often more catalytically active of the two.[11–14] The electron mobility of anatase is also much greater than the mobility of rutile.[15,16] It is known that defects and disorder[16–18] are important for electron mobility (reduced TiO_2 is an n-type conductor). An interesting observation is that a mixture of the two phases is more active for several reactions than the individual phases.[12,13,19,20] One proposed explanation for this increased catalytic behavior is that electrons selectively migrate from anatase to rutile, leading to an excess of holes on anatase.[21] The excess holes react with surface-adsorbed species, and a net increase in reaction rate is seen compared to anatase alone. Another theory proposes the opposite: electrons selectively migrate to anatase with a similar reaction increase on rutile.[22] Understanding the rate processes of electron mobility is thus important for quantifying and comparing the electrochemical activity of these phases.

As a long-term objective, we aim to obtain a comprehensive computational characterization of charge transport in titania that accounts for the varied crystalline structures, the role of crystalline defects, and the role of surfaces and interfaces. As a base line, it is important to validate the fundamental aspects of our theoretical characterization. The present work is the first step in this effort. It is completely focused on the determination of the intrinsic charge transport rates in perfect crystalline structures. As we will see below, the calculated rates obtained with our well established and benchmarked theoretical methodology are not in accord with the electron mobilities determined experimentally for rutile and anatase, in that we predict that the intrinsic polaron mobility in rutile is larger than the intrinsic polaron mobility in anatase. Our success in applying our computational methodology to hematite[23] and chromia[24] and in obtaining near quantitative agreement with experiment for these materials gives credence to our prediction for titania. This finding underscores the role of impurities, defects, phonons, surfaces, and interfaces in charge transport within titania, especially when comparing modeling results for this material with experimental data. In any case, our present work offers a firmly founded base line, and future work, to be undertaken and reported, will account for these factors one at a time.

We present in this work a computational characterization of negative polaron structures and intrinsic polaron hopping in both perfect bulk rutile and anatase. Dupuis and coworkers previously successfully modeled electron and hole

transport in chromia (α-Cr_2O_3),[24] hematite (α-Fe_2O_3),[23] and iron oxide[25] using a similar methodology to the one contained herein. Marcus theory[26,27] applied in the context of polaronic systems, such as metal-oxide solids, leads us to calculate activation energies and electronic coupling for polaron hopping, and thus polaron hopping rates and polaron mobility.

Emin[4(a)] and Holstein[4(b)] and Austin and Mott[4(c)] have given theoretical formulations for the description of polaron movement in solids. We note that several concepts in the Emin-Holstein-Austin-Mott theory (EHAM) and in Marcus theory bear resemblance in spite of their different terminology. In the review by Austin and Mott, it is notable that the diagram of the potential-energy surfaces for the initial and final states that enter the EHAM polaron hopping theory is identical to the Marcus diagram for electron transfer reproduced below. Both EHAM and Marcus consider the electronic states as residing in parabolic energy surfaces (see Fig. 2 of the text by Austin and Mott). Electronic coupling J in EHAM's theory is denoted by V_{AB} in Marcus' theory, and the activation energy is termed W_H in EHAM's theory rather than ΔG^* in Marcus' theory. While our starting point was Marcus theory, it is clear that, in the context of the present application and approximation, Marcus theory for polarons and the EHAM model are equivalent.

An overview of the formulation of Marcus theory used herein to characterize polaron hopping is given in Sec. II. Section III gives the details of our computational approach. Section IV gathers our results which allow a comparison of electron transport through rutile and anatase and further our understanding of the electrochemical differences between the two phases.

II. MODEL BACKGROUND

In what follows, negative polaron transfer is described as an alternation of cations in oxidation states 3 and 4. A schematic representation of the electronic structure of the states involved in a basic polaron transfer process is depicted in Fig. 1, which shows three relevant states. In equilibrium configuration q_A, the extra electron is localized on one particular Ti site and Ψ_A represents state Ti^{3+}-Ti^{4+}, while in configuration q_B, the electron has moved to an adjacent site and Ψ_B represents state Ti^{4+}-Ti^{3+}. The "transition" state between the two is designated as q_C. The labels q_A, q_B, and q_C are shorthand notations representing the polaronic configurations. An important element in Fig. 1 is the different sizes of the dots that represent the Ti atoms involved in the process. A larger dot is assigned to the metal atom carrying the extra electron and longer bonds are shown between the metal atom and the oxygen atoms bound to it, to reflect the "larger size" of the metal atom in the reduced oxidation state, as is commonly observed. Polaron transfer from state A to state C thus involves an antiphase (antisymmetric) breathing vibration mode around the reduced and oxidized sites. A linearized mathematical model of this polaronic distortion will be used below as a definition of the polaron transfer coordinate. To describe the transfer process, we make use of the EHAM theory or, in our case, the quasiequivalent Marcus theory, of which several reviews exist.[26,27]

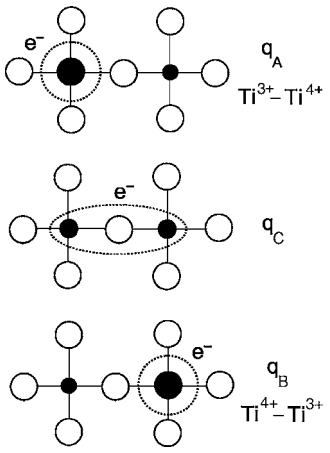

FIG. 1. Schematic diagram of polaron e^- transfer. In the initial state Ψ_A with structure q_A, the electron is localized on the left Ti ion, while in the final state Ψ_B with structure q_B, the electron is localized on the right Ti ion. At the transition state Ψ_C with structure q_C (a thermal transfer regime), the electron is shared between the two Ti ions.

Within these two theories, there are three important parameters: the reorganization energy λ, the diabatic activation energy ΔG^*, and the electronic coupling element V_{AB}. These parameters and the general features of the theories are illustrated in Fig. 2.

Under the Marcus-Emin-Holstein-Austin-Mott theories, the initial and final states are considered to be individual states that fluctuate about their equilibrium structures. The energy curves are assumed parabolic in shape. If an initial state has enough energy to surmount an activation barrier, then an electron may be transferred to an adjacent site and lead to the final state. The activation barrier depends strongly on the interaction between the initial and final states, which is quantified by the electronic coupling V_{AB}. In the absence of significant interaction between the initial and final states at q_C (small V_{AB}) the activation free energy is simply ΔG^*. This

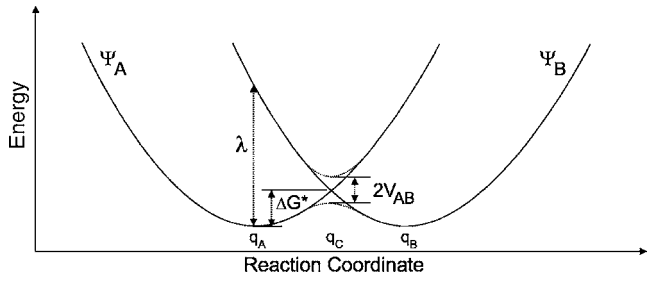

FIG. 2. General features of Marcus-Emin-Holstein-Austin-Mott theory for symmetric polaron transfer. The potential-energy surfaces of the initial state Ψ_A and final state Ψ_B are shown with equilibrium structures q_A and q_B. In our case, the initial state is Ti^{3+}-Ti^{4+} and the final state is Ti^{4+}-Ti^{3+}. The coincidence state, or transition state, between the two states is shown as q_C. The reorganization energy λ corresponds to the energy of the final state Ψ_B at the geometric configuration q_A. The diabatic activation energy is shown as ΔG^*. The adiabatic energy curves are shown as dashed lines, with the electronic coupling matrix element V_{AB} given as twice the energy difference between the two adiabatic states.

is known as a nonadiabatic or diabatic transfer, and the main mechanism for electron transfer occurs via quantum tunneling. If there is strong coupling (large V_{AB}), the activation barrier is lowered by the amount V_{AB}. This is the adiabatic case, and the main hopping mechanism occurs via thermal hopping. The other parameter, λ, is the reorganization energy and corresponds to the energy required to move, or reorganize, the electron to the site of the final state while retaining the initial state geometry. In the diabatic limit, the reorganization energy is $4\Delta G^*$.

Whether the polaron transfer is treated as adiabatic or diabatic is determined by the transmission probability κ. This transmission coefficient gives the probability of transfer from the initial state to the final state and is given by[28]

$$\kappa = \frac{2P_{12}^o}{(1+P_{12}^o)}. \tag{1}$$

The probability of conversion to the final state per passage through the intersection, P_{12}^o, is given below for the self-exchange process,[29] based on the work of Landau[30] and Zener,[31,32]

$$P_{12}^o = 1 - \exp[-(V_{AB}^2/h\upsilon_n)(\pi^3/\lambda k_B T)^{1/2}]. \tag{2}$$

In the above equation, υ_n is a typical frequency for nuclear motion. We used longitudinal optic-mode phonon frequencies for both rutile[33] and anatase,[34] giving $h\upsilon_n$ values of 0.10 and 0.11 eV for rutile and anatase, respectively. The specific phonon mode of interest here is the antiphase breathing mode of the oxygen atoms bound to the polaron's reduced site and of the oxygen atoms bound to the oxidized site to which the polaron transfers. When the two sites involved in the polaron transfer share bridging oxygen atoms, the phonon or vibration mode that corresponds to the transfer exhibits an asymmetric displacement of the bridging atoms. This is the mode that is captured in a linearized approximation of the polaron transfer coordinate, as described later. In any case, a value near 1 for κ indicates adiabatic transfer.

In the adiabatic case, the rate of polaron transfer is given as[29]

$$k_{et} = \upsilon_n \exp\left[\frac{-\Delta G_{ad}^*}{k_B T}\right]. \tag{3}$$

The adiabatic activation energy is

$$\Delta G_{ad}^* = \frac{\lambda}{4} - V_{AB}. \tag{4}$$

In contrast, the diabatic transfer rate is given by[26]

$$k_{et} = \frac{2\pi}{\hbar}|V_{AB}|^2 \frac{1}{\sqrt{4\pi\lambda k_B T}} \exp\left[-\frac{(\Delta G^o + \lambda)^2}{4\lambda k_B T}\right]. \tag{5}$$

For this work, all Ti sites are equivalent, so ΔG^o is zero. Beyond calculating the transfer rates, we can calculate the polaron mobility μ from the Einstein relation[35]

$$\mu = \frac{eD}{k_B T}. \tag{6}$$

The diffusion coefficient D is calculated from[36,37]

$$D = R^2 n k_{et}. \tag{7}$$

R in the above equation is the distance between transfer sites and n is the number of neighboring electronic accepting sites. In Sec. III below, we give the details of the calculations that we carried out to determine the parameters of the theory, mainly, the reorganization energy and the electronic coupling element.

III. COMPUTATIONAL METHODOLOGY

Spin-polarized density functional theory (DFT) with a plane-wave basis set, as implemented in the Vienna *ab initio* software package (VASP),[38–41] allowed the accurate modeling of polarons in bulk TiO_2. We described the core electrons using the projector augmented-wave method.[42] Two valence electron schemes for Ti were considered: $4s^2 3d^2$ (large core) and $3p^6 4s^2 3d^2$ (small core). Preliminary calculations determined that the former (large core) scheme was insufficient for obtaining the correct band gap, but tests showed that this scheme did give similar polaron transfer rates to the small core model. Nonetheless, we used the $3p^6 4s^2 3d^2$ scheme for our calculations to ensure proper description of valence electrons. The oxygen atoms had valence configurations of $2s^2 2p^4$. The exchange-correlation functional for this work was the functional of Perdew *et al.*[43,44]

It is important to ensure convergence of simulation parameters. We therefore tested our k-point meshes ($2\times2\times2$ for rutile and $2\times2\times1$ for anatase) and cutoff energies and found them to be sufficiently converged. We also used Gaussian smearing to describe the electronic occupation. The cells that we considered were the rutile ($3\times3\times3$) and anatase ($3\times3\times2$) supercells. These cells have 162 and 216 atoms, respectively, and are shown in Fig. 3. Our calculations gave lattice parameters of 4.65 and 2.97 Å for rutile and 3.81 and 9.73 Å for anatase, all in good agreement with experiment.[45] This leads to simulation box lengths of 14.01 Å and 8.91 Å for the rutile cell and 11.46 Å and 19.42 Å for the anatase cell. We also tested a ($4\times4\times4$) rutile cell and found little effect on the results (for example, Ti-O distance, E_{act}, etc.).

The method for determining the polaron structures involved adding an extra electron to bulk supercells while employing the DFT+U level of theory, and then allowing the systems to relax in response to this extra electron. This relaxed system effectively modeled the polaron structure.

One problem encountered using DFT is that correlation effects can lead to errors in the calculations. The underprediction of the band gap in semiconductors is a well-known difficulty. We also experienced problems with DFT in describing the polaron structures. The extra electron added to a system described by DFT became delocalized throughout the cell and was not confined to any particular Ti ion. This is a well-known deficiency of DFT, a manifestation of the self-interaction of unpaired electrons in functionals of the density in the generalized gradient approximation. Several approaches in correcting for electron self-interaction have been proposed, including the definition and inclusion of a self-interaction correction term, or the *ad hoc* mixing of a frac-

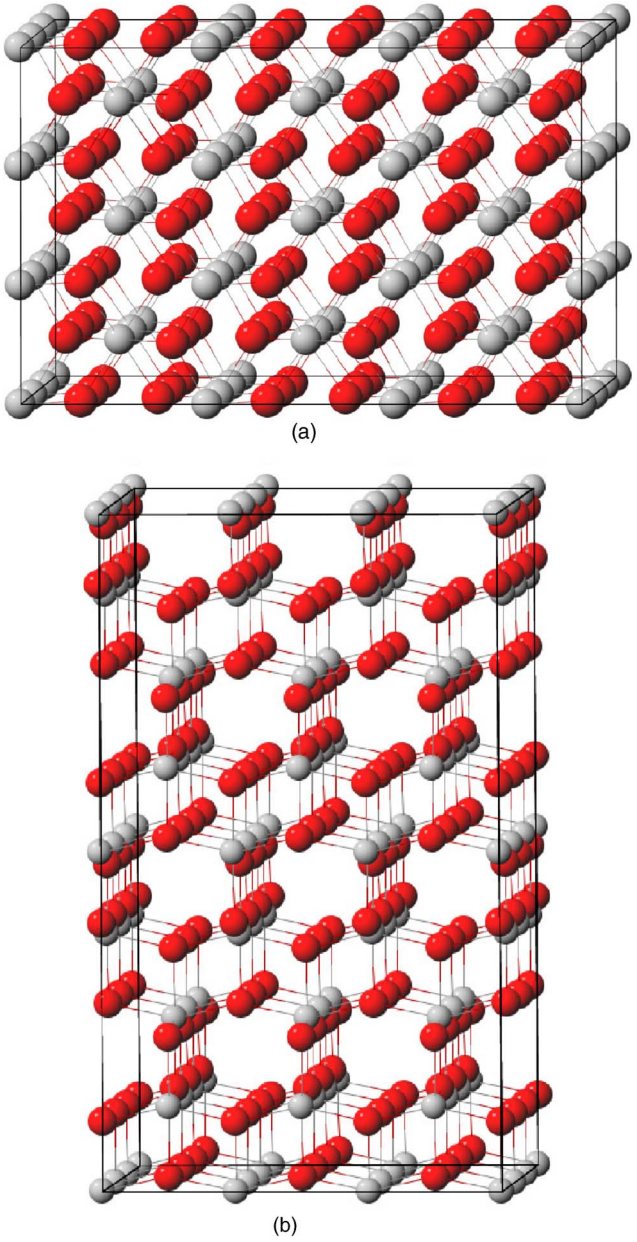

FIG. 3. (Color online) Bulk structures of TiO_2 relevant to this study. (a) $3\times3\times3$ rutile supercell. (b) $3\times3\times2$ anatase supercell. Ti atoms are depicted as gray spheres, while O atoms red spheres.

tion of the exact Hartree-Fock exchange (a very popular approach in chemistry), or, finally, the inclusion of a Hubbard-like U correction term in the Kohn-Sham operator that reduces self-interaction errors.

This last method is the DFT+U method of Liechtenstein *et al.*,[46] and we made use of it for our work. A similar method was used by Maxisch *et al.*[47] to describe polaron transfer in Li_xFePO_4. Within this framework, the parameters U (Coulomb interaction) and J (exchange interaction) become the main determining factors for the magnitude of the correction. There is of course no universal value of U that makes DFT+U work equally well for all systems. A common approach in finding the "optimal" parameters for a given system is to fix J and vary the U value. Analysis of

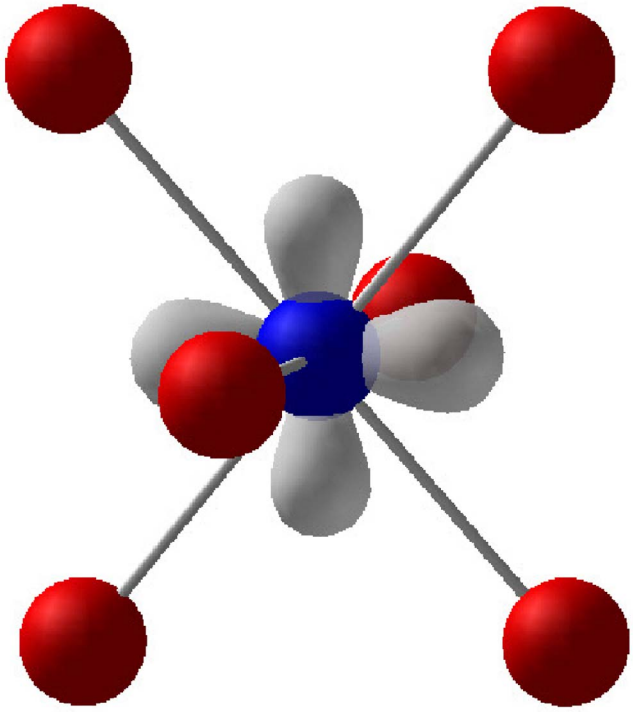

FIG. 4. (Color online) Charge-density difference plot of polaron structure in rutile. The charge difference is taken between the cell with an extra electron and the cell without an extra electron. The density plot is shown for an isocharge of 0.176 $e^-/Å^3$.

properties of interest as a function of the effective U value ($U_{\text{eff}}=U-J$) suggests the appropriate parameters. We chose a J value of 1 eV for our work. We detail our efforts to find an optimal U_{eff} under Sec. IV.

Verification of the polaron structure is necessary to validate our simulation technique. We performed Bader's atoms in molecule charge analysis[48] using the program of Henkelman *et al.*[49] The charges in the $(3\times3\times3)$ rutile cell were found to be +2.2 for the Ti polaron site, compared to a charge of +2.6 for the nonpolaron Ti ions. In addition, a plot of the charge-density difference of the $(3\times3\times3)$ rutile cell with and without an extra electron is given in Fig. 4. As can be seen, the extra electron localizes in a t_{2g} state on the Ti ion. We also examined the density of states and verified that the extra added electron filled d states.

The correct localization of electrons allows calculation of activation energies and reorganization energies according to the following description. With the electron localized on an initial and final site, we used a linear interpolation scheme to calculate the polaron transfer pathway,

$$q(x) = xq_A + (1-x)q_B. \tag{8}$$

q_A, q_B, and q_C are vectors of the three-dimensional coordinates of all the atoms in the unit cell. In Eq. (8), x varies between 0 and 1, $0\leqslant x\leqslant 1$. $x=1$ corresponds to the final state, $x=0$ corresponds to the initial state, and $x=0.5$ corresponds to the transition state that happens to be the midpoint, owing to the translational equivalence of the final and initial states. This approach has been shown[50] to give a good rep-

resentation of the polaron transfer coordinates in our earlier work on other metal oxides. The linearization of the coordinates proved to be acceptable in these earlier cases and we expect it to work equally well in the present case owing to the small changes in Ti-O bond distances associated with the polaron distortion and hopping. As we mentioned earlier, this linearized coordinate captures the physics of the key phonon mode associated with the polaron transfer, the antiphase breathing polaronic expansion around the reduced metal site, and the contraction around the oxidized metal site. The energy of the structure at q_C is taken as the transition state E_{act} or crossing-point free energy, depending on the regime, nonadiabatic or thermal, of the polaron transfer. We assumed the enthalpic and entropic changes of the free energy to be negligible, which is typical for solid-state calculations. We evaluated the reorganization energy as $4\Delta G^*$, assuming parabolic potential-energy surfaces. That this is indeed the case will be illustrated later.

Currently, calculation of the coupling element V_{AB} is not possible with VASP, but such a calculation is feasible with the molecular code NWCHEM.[51,52] NWCHEM contains a module, based on the method of Farazdel *et al.*,[50] for calculating the electronic coupling. The formula used for this calculation is

$$V_{AB} = \frac{|H_{AB} - S_{AB}(H_{AA} + H_{BB})/2|}{1 - S_{AB}^2}, \tag{9}$$

with $H_{AB}=\langle\Psi_A|H|\Psi_B\rangle$ and $S_{AB}=\langle\Psi_A|\Psi_B\rangle$. We used cluster models for this work and extracted these clusters from the converged supercell periodic structures. In these clusters, we terminated the appropriate oxygen ions with hydrogen atoms along Ti-O bond lengths to maintain charge neutrality. The O-H distances were fixed at 0.96 Å when we performed these static calculations. We considered several cluster sizes, which we detail in Sec. IV. These calculations were performed at the unrestricted Hartree-Fock level with 6-311G basis sets[53] for O and H and the Ahlrichs VTZ basis set[54] for Ti.

IV. RESULTS AND DISCUSSION

A. Nonadiabatic activation energies from periodic calculations

Determination of an appropriate U parameter is necessary for DFT+U calculations in order to correct the electron self-interaction in DFT. There is no universal U value that works equally well for all materials or for all properties of interest. For example, recent papers show how the choice of U affects various properties of CeO_2.[55,56] A typical approach is to examine how U affects a property of interest, such as defect formation energy or band-gap energy, and use these results as a guide for careful choice of U. We therefore first chose to examine how the band gap was affected by our choice of U. Experimentally, the band gap has been found to be near 3.0 eV for rutile[57] and near 3.2 eV for anatase.[58] Our results, summarized in Fig. 5, show that a U_{eff} value near 10.0 eV gives band gaps in satisfactory accord with experiment. A similar value of U was obtained by Persson and da Silva,[59] adding credence to this value. We further examined how U_{eff} affects the activation energy of polaron transfer before finalizing a U_{eff} value for our work.

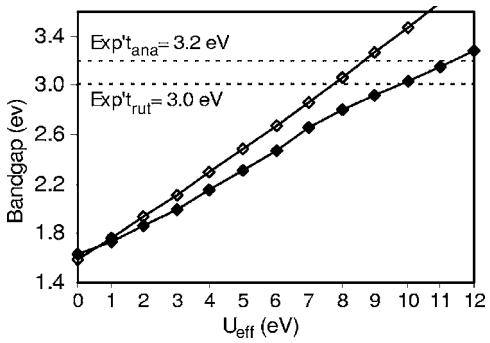

FIG. 5. Band gap versus U_{eff}. Closed diamonds represent results for rutile, while open diamonds represent results for anatase.

A scheme must be developed to describe the different negative polaron transfer possibilities. Every Ti atom in perfect bulk rutile and anatase is symmetrically equivalent, so we only considered polaron transfer from one particular Ti atom per supercell. We localized the polaron at the origin of the cell (0,0,0) and then transferred it to an adjacent site. Any originating site could be considered and would give the same results. In rutile, we studied two different polaron transfer directions, both toward the two closest neighboring Ti atoms. Similarly, there are two different closest Ti neighbors in anatase leading to two transfer directions. Figure 6 shows the possibilities for these transfers. In rutile, the electron may move along the [001] or [111] direction, while in anatase, the electron may move along the [100] or [201] direction. The [001] direction in rutile is parallel to the c direction, while the [100] direction in anatase is parallel to the a direction. These directions represent families of directions that can occur in the bulk. For example, electron transfer along [111] in rutile would also be representative of transfer along $[\bar{1}11]$, $[1\bar{1}1]$, and $[11\bar{1}]$.

With a transfer scheme defined, calculation of the activation energies for the various processes is now possible. As mentioned in Sec. III, we considered a linear interpolation method to define the transfer pathway. Figure 7 shows typical results of this method along the [001] direction in the $(3\times3\times3)$ rutile cell. Both final and initial states have the same energy, and the transfer pathway is symmetric about the transition state, or quasidiabatic crossing state. The energy curve shown in Fig. 7 exhibits a cusp at the midpoint, and we assign this behavior to a nonadiabatic polaron transfer. The curve is parabolic ($R^2=1.00$ from fitting), attesting that Marcus theory is appropriate for this transfer process. We also tested how U_{eff} affected the activation energy. Figure 8 shows these results along the [001] direction in the $(3\times3\times3)$ rutile cell. The graph suggests that the crossing-point energy saturates at a U_{eff} value near 10 eV, indicating that we have reached full localization (as opposed to partial delocalization) in the extra d orbital. All remaining calculations are therefore performed with the U_{eff} value of 10 eV.

This value of U seems large, but also highlights the difficulty in choosing an appropriate U value. While methods exist to predict U values self-consistently, such methods tend to give U values different than those predicted from property matching.[56] Indeed, the appropriate value of U depends

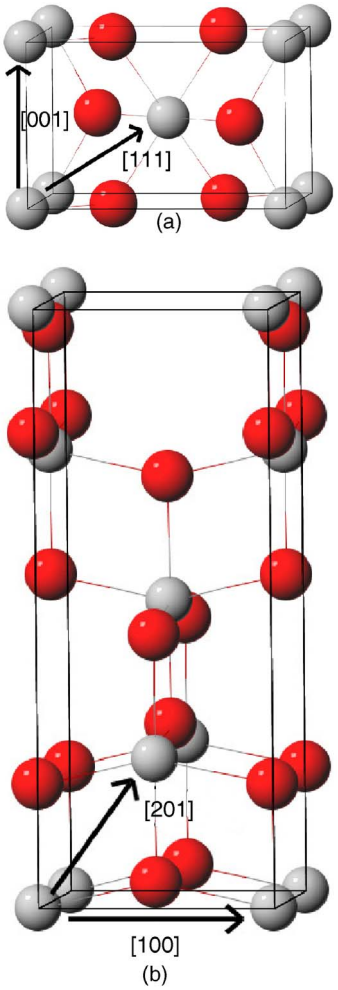

FIG. 6. (Color online) Negative polaron transfer directions for (a) bulk rutile and (b) bulk anatase. The localized electron (polaron) moves to an adjacent Ti atom in all cases.

strongly on the property of interest.[55,56] Within the DFT+U framework, there is no way to predict a "correct" value of U that will match every property. In our case, we are trying to localize an electron on a 3d transition metal, and to achieve this, a large U value is needed to overcome the tendency of the excited electron to delocalize due to self-interaction errors.

The results for the different activation energies and reorganization energies are summarized in Table I. All of the

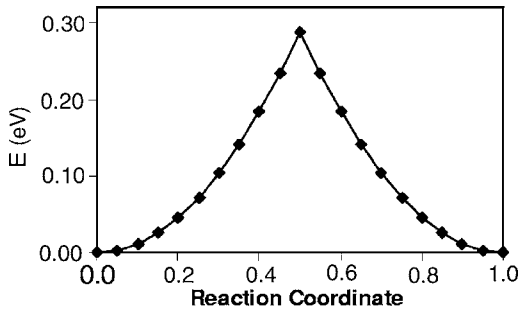

FIG. 7. Electron transfer energies along the [001] direction in bulk rutile for U_{eff}=10 eV.

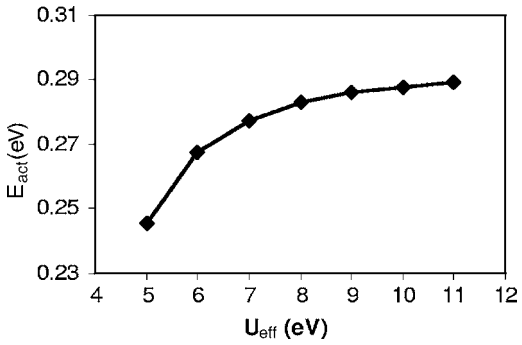

FIG. 8. Crossing-point energies versus U_{eff}. Results are shown along the [001] direction for rutile.

crossing-point activation energies are near 0.3 eV with reorganization energies near 1.2 eV. The observation of energies that are similar along different directions was also observed by Iordanova *et al.*[24] in their work with Cr_2O_3. We attribute the similarity in the energies to similar geometries of rutile and anatase, and the similar phonon structure of rutile and anatase. In both rutile and anatase, the Ti have octahedral geometries with similar Ti-O and Ti-Ti distances. Comparing the phonon structures, rutile has frequencies[33] of 811, 806, 500, and 458 cm^{-1}, while anatase has frequencies[34] of 876, 755, 435, and 367 cm^{-1}. The similar phonon frequencies are indicative that the initial states will leave their respective energy wells at similar rates due to similar energy curvature. The small differences in energies can be correlated with Ti-Ti and Ti-O distances. In rutile, the smallest activation energy is 0.288 eV along the [001] direction, while an activation energy of 0.307 eV occurs along the [111] direction. The bulk Ti-Ti distances are 2.970 Å along [001] and 3.610 Å along [111]. The bulk Ti-O distances are 1.963 Å for transfer along [001] and 2.007 Å along [111]. Shorter distances between transfer sites therefore correlate with smaller activation energies. Similar analysis can be applied and shown for anatase. The effect, however, is very small.

Formation of a polaron causes a reorganization of the local geometry around the Ti^{3+} site. In Table II, we give the interatomic distances at the Ti site with and without an extra electron. Figure 9 displays the Ti-O bond length changes near the polaron relative to the structure without a polaron. The figure indicates that the geometrical changes are largely centered near the polaron, indicative of small-polaron formation. Upon formation of a polaron, the Ti-Ti distances typically change very little, at most 0.006 Å. Greater changes

TABLE I. Nonadiabatic activation energies for polaron transfer.

Phase	Direction	E_{act} (eV)	E_{reorg} (eV)
Rutile	[001]	0.288	1.152
	[111]	0.307	1.229
Anatase	[100]	0.304	1.214
	[201]	0.297	1.188

TABLE II. Ti-Ti and Ti-O distances at the polaron site.

Phase	Direction	Ti-Ti distance (Å)	Closest Ti-O distance (Å)
Rutile	[001]	2.970	1.973
	[111]	3.611	1.992
Rutile with polaron	[001]	2.966	2.068
	[111]	3.611	2.029
Anatase	[100]	3.808	1.947
	[201]	3.088	2.025/1.947
Anatase with polaron	[100]	3.802	1.982
	[201]	3.090	2.179/1.982

can be seen in the Ti-O distances, though most of these changes are still small, between 0.154 and 0.035 Å. We ascribe the increased Ti-O bond lengths to the partial electron-density filling of antibonding orbitals formed by mixing Ti and O atomic orbitals. Filling antibonding orbitals decreases bond stability, which is reflected by the longer Ti-O distances near the polaron. These results are consistent with the earlier

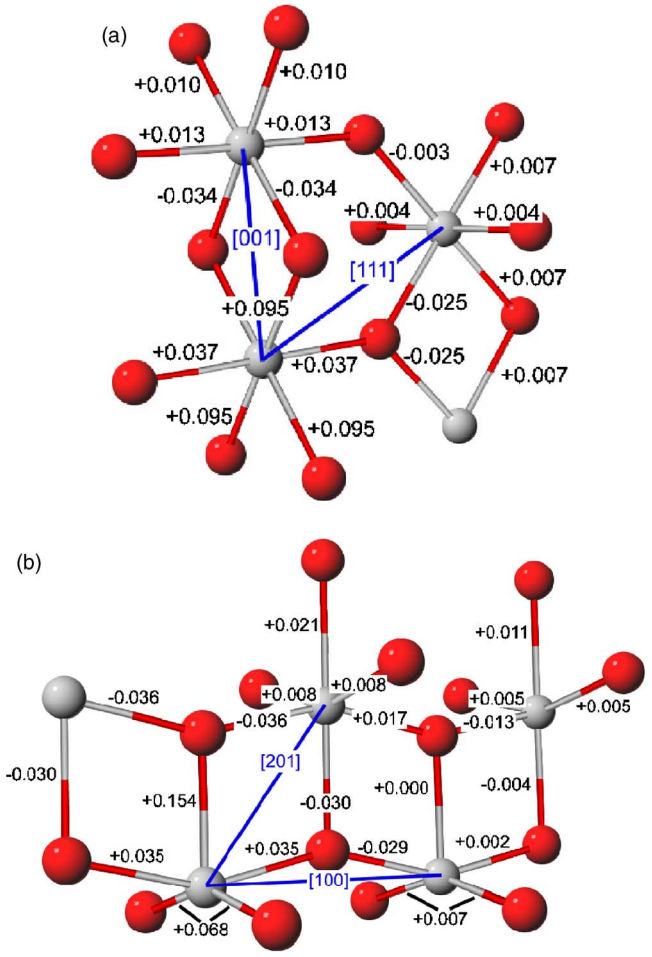

FIG. 9. (Color online) Geometry changes induced upon polaron formation in (a) rutile and (b) anatase. All numbers are given in Å.

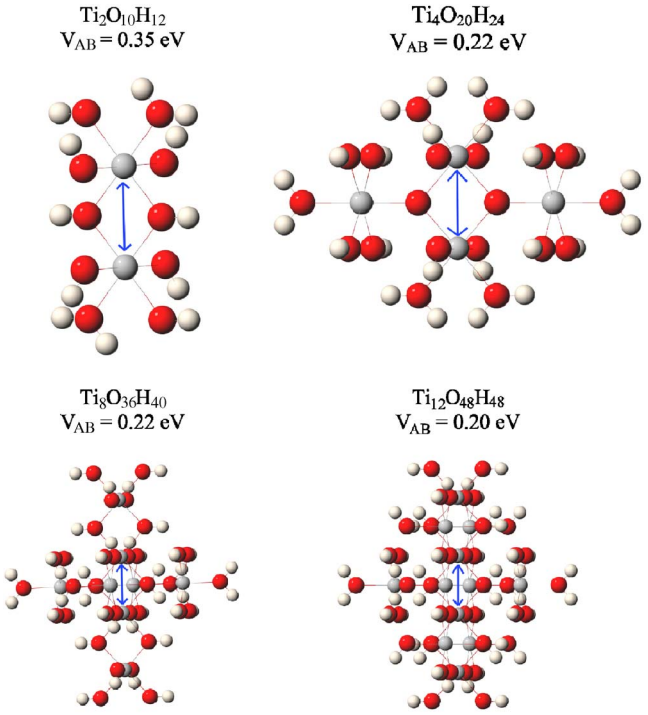

FIG. 10. (Color online) Clusters for V_{AB} calculations along [001] in rutile.

description of the formation of a polaron involving the breathing vibrational mode around the reduced site, and of polaron transfer involving the antiphase breathing mode around the reduced site and the oxidized sites in the polaron transfer. We note that analysis of the charges for both rutile and anatase shows them to be closer than the oxidation states +3 and +4 would suggest: +2.2 for the Ti^{3+} site and +2.6 for the Ti^{4+} sites. The Ti cations in rutile and anatase are in similar O_h environments, so they exhibit similar electronic behavior.

B. Electronic coupling from cluster calculations

We extracted clusters from the converged supercell periodic polaron structures for the calculation of the electronic couplings V_{AB} at the crossing point. In Fig. 10, we show typical clusters used for the electronic coupling calculations, these being for transfer along [100] in rutile. These clusters range in size from Ti_2 to Ti_{12} clusters. Our results show that the clusters are generally converged with the Ti_4 cluster and simple dimers were not large enough to obtain V_{AB} values that are converged with respect to cluster size. We obtained values of V_{AB} of 0.35 eV for Ti_2, 0.22 eV for Ti_4 and Ti_8, and 0.20 eV for Ti_{12}. The clusters for transfer along [111] gave very different results. For the Ti_2 and Ti_6 clusters, we obtained V_{AB} values of 0.00 and 0.02 eV, respectively. We tested a large Ti_{18} cluster that essentially was a Ti dimer fully surrounded by Ti atoms and obtained a V_{AB} value of 0.01 eV. These results indicate that very large clusters are not needed to reach convergence of the electronic coupling element. We also calculated the V_{AB} terms for the anatase structures and obtained values of 0.02 eV along the [100] transfer and

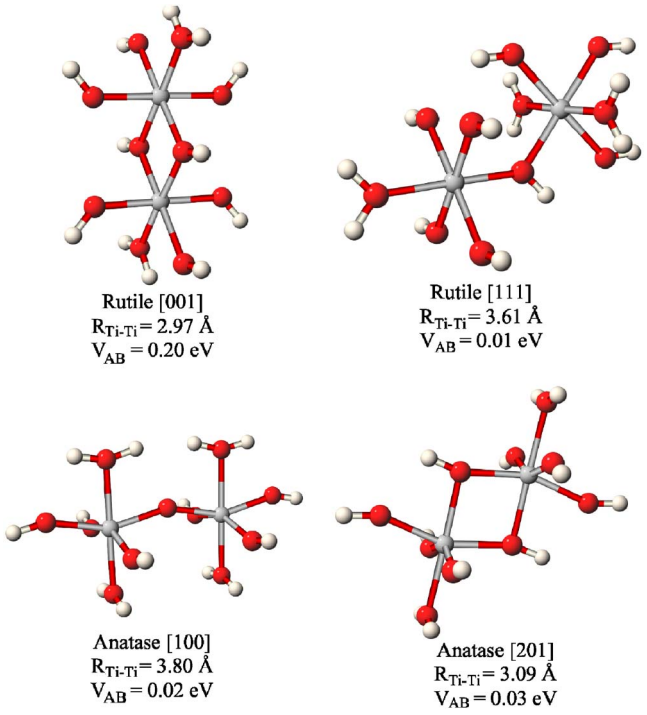

FIG. 11. (Color online) Cluster structures for the V_{AB} calculations.

0.03 eV along the [201] transfer. These were calculated from Ti_9 and Ti_8 clusters, respectively.

The different V_{AB} results for the different directions and phases elicit explanation. We attribute the differences in V_{AB} values to three factors: the Ti-Ti distance, the degree of O bridging, and orientation of *d* orbitals. In Fig. 11, we show the simplest clusters used in these calculations with the Ti-Ti distances and V_{AB} values indicated. Transfers along the [001] and [111] directions for rutile involved a Ti-Ti distance of 2.97 Å with two bridging oxygen atoms and a Ti-Ti distance of 3.61 Å with a single bridging oxygen, respectively. The [100] and [201] directions in anatase involved a Ti-Ti distance of 3.80 Å and one bridging oxygen and a Ti-Ti distance of 3.09 Å with two bridging oxygens, respectively. The rutile [001] transfer coupling element is the largest at 0.20 eV corresponding to a Ti-Ti distance of 2.97 Å. The rutile [111] coupling element is much smaller at 0.01 eV with a Ti-Ti distance of 3.61 Å. These results are consistent with the well accepted (exponential) decay of the electronic coupling with distance. Interestingly, for rutile [001] and anatase [201], the Ti-Ti distances are rather similar but the

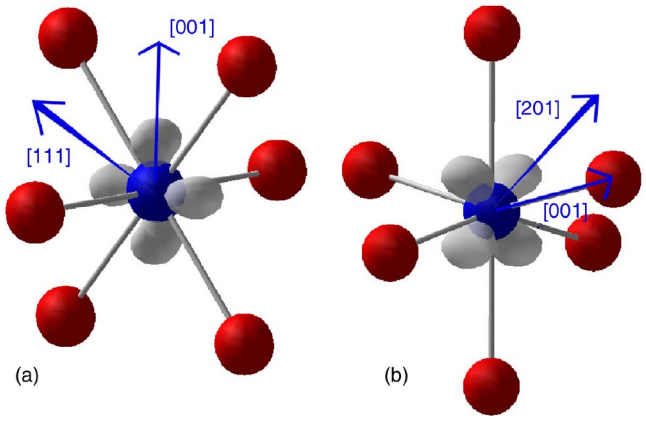

FIG. 12. (Color online) Orientation of *d* orbitals in (a) rutile and (b) anatase. The orbitals are obtained from charge-density difference analysis of the structures with and without an extra electron.

electronic couplings differ by 1 order of magnitude. Bridging ligand atoms are known to contribute to the magnitude of the electronic coupling by providing orbitals that assist in the charge transfer (superexchange mechanism). The disparities in distances amongst the rutile directions and amongst the anatase directions do not allow a differentiation of the superexchange contributions of the bridging atoms to the electronic coupling. Consideration of rutile [001] and anatase [201] with similar Ti-Ti distances and the same number of bridging oxygens suggest that other factors contribute strongly to the electronic coupling. Analysis of the polaronic wave functions in their initial and final states reveals the effect due to the atomic states of the polarons.

Analysis of the *d* orbitals provides additional insight into the variations in magnitude among the V_{AB} values. Figure 12 shows charge-density difference plots of the rutile and anatase systems with polaron transfer directions shown. As indicated, the polaron orbitals are oriented along the transfer direction for the rutile [001] transfer. The other three transfers, however, do not have the polaronic orbitals oriented along the transfer direction. This alignment of orbitals in rutile [001] contributes to greater overlap of the initial and final localized states and hence larger V_{AB}.

C. Polaron transfer rates

With the reorganization energy and electronic coupling parameters, rates of polaron transfer can be calculated using Eqs. (1)–(7). These calculations are summarized in Table III. The calculated κ values show that polaron transfer is adia-

TABLE III. Electron transfer rates and associated parameters.

Phase	Direction	ΔG^* (eV)	K	Transfer mode	k_{et} (s^{-1})	D (cm^2/s)	μ ($cm^2/V\,s$)
Rutile	[001]	0.09	1.00	Adiabatic	7.65×10^{11}	1.35×10^{-3}	5.24×10^{-2}
	[111]	0.31	0.02	Nonadiabatic	3.66×10^{6}	1.91×10^{-8}	7.42×10^{-7}
Anatase	[100]	0.30	0.17	Nonadiabatic	3.68×10^{7}	2.71×10^{-7}	1.06×10^{-5}
	[201]	0.30	0.45	Nonadiabatic	1.73×10^{8}	1.27×10^{-6}	4.96×10^{-5}

batic along rutile [001] and nonadiabatic along the other directions. Predictably, the results also show that the rate of transfer and mobilities are largest along rutile [001], which results directly from the lower ΔG^* which, in turn, results from the larger V_{AB} value. The mobility and diffusion constants are correspondingly largest for rutile [001]. We need to emphasize again here that what we calculated here are intrinsic diffusional mobilities for the two crystalline structures of titania, along specific directions. In contrast, experimentally measured mobilities are typically drift or Hall mobilities. Thus, the calculated quantities are not directly comparable to the experimental values. A more complete model would have to include several other features, such as effects associated with the photoexcitation wavelength, structural defects and disorder, or applied voltage effects. Nevertheless, an activation energy derived from drift mobility data along rutile [001] was found to be 0.07 eV,[4,5] in satisfactory accord with our calculated activation energy.

V. CONCLUSIONS

We have calculated several parameters that enter the Emin-Holstein-Austin-Mott theory and the quasiequivalent Marcus theory for polaron transfer in rutile and anatase TiO_2. We showed that use of DFT+U yields localization of an electron at a Ti site, leading to polaron formation. A U_{eff} value of 10.0 eV gave band-gap values that agreed well with experimentally measured band gaps and was used for this work. Diabatic activation energies for the transfer were calculated to be near 0.3 eV in both rutile and anatase. The fact that both rutile and anatase have comparable activation energies is attributed to similar local structures with octahedral environment of the Ti sites and similar phonon frequencies. We also calculated the electronic coupling V_{AB} which exhibited a much larger value for transfer in rutile, 0.20 eV, compared to transfer in anatase, 0.03 eV. The results show the well established effect of the distance dependence of the electronic coupling. We found no clear differentiation of the superexchange contribution due to the bridging oxygen atoms, one or two, between Ti sites involved in polaron transfer. From our calculations, we have evidence of the effect on the electronic coupling element of the orientation of the d atomiclike orbitals in the initial and final states of the polaron transfer, with the larger coupling when the d orbitals have favorable overlap. Our results show the most favorable polaron transfer to be adiabatic in rutile and diabatic in anatase, with a much larger transfer rate in rutile. An adiabatic activation energy of 0.09 eV in rutile is in satisfactory agreement with experimental results.

This work has focused on the intrinsic electron transport properties of rutile and anatase. We have applied a computational methodology that has proven successful for other oxides. This work predicts that intrinsic electron transport in bulk titania is faster in rutile than in anatase. This finding is in contrast with experimental measurements that suggest that electron transport in anatase is more facile, and we assign this difference to other effects not accounted for in the present work: structural defects, applied voltage, or photoexcitation which are believed to greatly affect polaron mobility in titania. The present work lays the groundwork for further development toward an atomic-level characterization of polaron transport in titania that would include also hole transport, electron-hole interaction and recombination, and effects of defects, surfaces, and interfaces.

ACKNOWLEDGMENTS

We wish to acknowledge Sebastien Kerisit and Kevin Rosso for useful discussions. Funding was provided by the Department of Energy, Office of Basic Energy Sciences. Computational resources were provided by the Molecular Science Computing Facility located at the Environmental Molecular Science Laboratory in Richland, WA. All work was performed at Pacific Northwest National Laboratory (PNNL). Battelle operates PNNL for the U.S. Department of Energy.

[1] O. Carp, C. L. Huisman, and A. Reller, Prog. Solid State Chem. **32**, 33 (2004).
[2] A. L. Linsebigler, G. Q. Lu, and J. T. Yates, Chem. Rev. (Washington, D.C.) **95**, 735 (1995).
[3] K. Kalyanasundaram and M. Gratzel, Coord. Chem. Rev. **177**, 347 (1998).
[4] (a) D. Emin and T. Holstein, Ann. Phys. (N.Y.) **53**, 439 (1969); (b) T. Holstein, *ibid.* **281**, 725 (2000); (c) I. G. Austin and N. F. Mott, Adv. Phys. **50**, 757 (2001). (d) This latter work by Austin and Mott provides a good overview of the previous work by Emin and Holstein.
[5] V. N. Bogomolov, E. K. Kudinov, and Y. A. Firsov, Sov. Phys. Solid State **9**, 2502 (1968).
[6] V. N. Bogomolov, E. K. Kudinov, D. N. Mirlin, and Y. A. Firsov, Sov. Phys. Solid State **9**, 1630 (1968).
[7] E. Yagi, R. R. Hasiguti, and M. Aono, Phys. Rev. B **54**, 7945 (1996).
[8] J. Nowotny, M. Radecka, and M. Rekas, J. Phys. Chem. Solids **58**, 927 (1997).
[9] P. K. Schelling and J. W. Halley, Phys. Rev. B **62**, 3241 (2000).
[10] J. Nelson and R. E. Chandler, Coord. Chem. Rev. **248**, 1181 (2004).
[11] A. Fujishima and X. T. Zhang, C. R. Chim. **9**, 750 (2006).
[12] M. C. Yan, F. Chen, J. L. Zhang, and M. Anpo, J. Phys. Chem. B **109**, 8673 (2005).
[13] C. Y. Wu, Y. H. Yue, X. Y. Deng, W. M. Hua, and Z. Gao, Catal. Today **93-95**, 863 (2004).
[14] M. Inagaki, R. Nonaka, B. Tryba, and A. W. Morawski, Chemosphere **64**, 437 (2006).
[15] L. Forro, O. Chauvet, D. Emin, L. Zuppiroli, H. Berger, and F. Levy, J. Appl. Phys. **75**, 633 (1994).
[16] R. G. Breckenridge and W. R. Hosler, Phys. Rev. **91**, 793 (1953).
[17] T. Dittrich, J. Weidmann, F. Koch, I. Uhlendorf, and I. Lauermann, Appl. Phys. Lett. **75**, 3980 (1999).

[18] A. Weibel, R. Bouchet, and P. Knauth, Solid State Ionics **177**, 229 (2006).
[19] T. Ohno, K. Sarukawa, K. Tokieda, and M. Matsumura, J. Catal. **203**, 82 (2001).
[20] T. Ohno, K. Tokieda, S. Higashida, and M. Matsumura, Appl. Catal., A **244**, 383 (2003).
[21] T. Kawahara, Y. Konishi, H. Tada, N. Tohge, J. Nishii, and S. Ito, Angew. Chem., Int. Ed. **41**, 2811 (2002).
[22] D. C. Hurum, A. G. Agrios, K. A. Gray, T. Rajh, and M. C. Thurnauer, J. Phys. Chem. B **107**, 4545 (2003).
[23] N. Iordanova, M. Dupuis, and K. M. Rosso, J. Chem. Phys. **122**, 144305 (2005).
[24] N. Iordanova, M. Dupuis, and K. M. Rosso, J. Chem. Phys. **123**, 074710 (2005).
[25] K. M. Rosso and M. Dupuis, J. Chem. Phys. **120**, 7050 (2004).
[26] R. A. Marcus and N. Sutin, Biochim. Biophys. Acta **811**, 265 (1985).
[27] R. A. Marcus, Rev. Mod. Phys. **65**, 599 (1993).
[28] J. Ulstrup, *Lecture Notes in Chemistry* (Springer, New York, 1979), Vol. 10, p. 89.
[29] B. S. Brunschwig, J. Logan, M. D. Newton, and N. Sutin, J. Am. Chem. Soc. **102**, 5798 (1980).
[30] L. Landau, Phys. Z. Sowjetunion **2**, 24 (1932).
[31] C. Zener, Proc. R. Soc. London, Ser. A **137**, 696 (1932).
[32] C. Zener, Proc. R. Soc. London, Ser. A **140**, 660 (1933).
[33] S. P. S. Porto, P. A. Fleury, and T. C. Damen, Phys. Rev. **154**, 522 (1967).
[34] R. J. Gonzalez, R. Zallen, and H. Berger, Phys. Rev. B **55**, 7014 (1997).
[35] A. Einstein, *Investigations on the Theory of the Brownian Movement* (Dover, New York, 1956).
[36] R. R. Heikes and W. D. Johnston, J. Chem. Phys. **26**, 582 (1957).
[37] J. B. Goodenough, in *Progress in Solid State Chemistry*, edited by H. Reiss (Pergamon, New York, 1971), Vol. 5, p. 145.
[38] G. Kresse and J. Furthmuller, Comput. Mater. Sci. **6**, 15 (1996).
[39] G. Kresse and J. Furthmuller, Phys. Rev. B **54**, 11169 (1996).
[40] G. Kresse and J. Hafner, Phys. Rev. B **47**, 558 (1993).
[41] G. Kresse and J. Hafner, Phys. Rev. B **49**, 14251 (1994).
[42] G. Kresse and D. Joubert, Phys. Rev. B **59**, 1758 (1999).
[43] J. P. Perdew, K. Burke, and M. Ernzerhof, Phys. Rev. Lett. **77**, 3865 (1996).
[44] J. P. Perdew, K. Burke, and M. Ernzerhof, Phys. Rev. Lett. **78**, 1396 (1997).
[45] C. J. Howard, T. M. Sabine, and F. Dickson, Acta Crystallogr., Sect. B: Struct. Sci. **47**, 462 (1991).
[46] A. I. Liechtenstein, V. I. Anisimov, and J. Zaanen, Phys. Rev. B **52**, R5467 (1995).
[47] T. Maxisch, F. Zhou, and G. Ceder, Phys. Rev. B **73**, 104301 (2006).
[48] R. F. W. Bader, Acc. Chem. Res. **18**, 9 (1985).
[49] G. Henkelman, A. Arnaldsson, and H. Jonsson, Comput. Mater. Sci. **36**, 354 (2006).
[50] A. Farazdel, M. Dupuis, E. Clementi, and A. Aviram, J. Am. Chem. Soc. **112**, 4206 (1990).
[51] E. Aprà, T. L. Windus, T. P. Straatsma, E. J. Bylaska, W. de Jong, S. Hirata, M. Valiev, M. Hackler, L. Pollack, K. Kowalski, R. Harrison, M. Dupuis, D. M. A. Smith, J. Nieplocha, V. Tipparajua, M. Krishnan, A. A. Auer, E. Brown, G. Cisneros, G. Fann, H. Fruchtl, J. Garza, K. Hirao, R. Kendall, J. Nichols, K. Tsemekhman, K. Wolinski, J. Anchell, D. Bernholdt, P. Borowski, T. Clark, D. Clerc, H. Dachsel, M. Deegan, K. Dyall, D. Elwood, E. Glendening, M. Gutowski, A. Hess, J. Jaffe, B. Johnson, J. Ju, R. Kobayashi, R. Kutteh, Z. Lin, R. Littlefield, X. Long, B. Meng, T. Nakajima, S. Niu, M. Rosing, G. Sandrone, M. Stave, H. Taylor, G. Thomas, J. van Lenthe, A. Wong, and Z. Zhang, NWCHEM, Pacific Northwest National Laboratory, Richland, Washington, 2005.
[52] R. A. Kendall, E. Apra, D. E. Bernholdt, E. J. Bylaska, M. Dupuis, G. I. Fann, R. J. Harrison, J. L. Ju, J. A. Nichols, J. Nieplocha, T. P. Straatsma, T. L. Windus, and A. T. Wong, Comput. Phys. Commun. **128**, 260 (2000).
[53] R. Krishnan, J. S. Binkley, R. Seeger, and J. A. Pople, J. Chem. Phys. **72**, 650 (1980).
[54] A. Schafer, H. Horn, and R. Ahlrichs, J. Chem. Phys. **97**, 2571 (1992).
[55] D. A. Andersson, S. I. Simak, B. Johansson, I. A. Abrikosov, and N. V. Skorodumova, Phys. Rev. B **75**, 035109 (2007).
[56] C. Loschen, J. Carrasco, K. M. Neyman, and F. Illas, Phys. Rev. B **75**, 035115 (2007).
[57] J. Pascual, J. Camassel, and H. Mathieu, Phys. Rev. B **18**, 5606 (1978).
[58] H. Tang, H. Berger, P. E. Schmid, F. Levy, and G. Burri, Solid State Commun. **87**, 847 (1993).
[59] C. Persson and A. F. da Silva, Appl. Phys. Lett. **86**, 231912 (2005).